3-D Monte Carlo-based Scatter Compensation in Quantitative I-131 SPECT Reconstruction

Yuni K. Dewaraja, Member, IEEE, Michael Ljungberg, Member, IEEE, and Jeffrey A. Fessler, Member, IEEE

***Abstract*- we have implemented highly accurate Monte Carlo based scatter modeling (MCS) with 3-D ordered subsets expectation maximization (OSEM) reconstruction. The scatter is included in the statistical model as an additive term and attenuation and detector response are included in the forward/backprojector. In the present implementation of MCS, a simple multiple window-based estimate is used for the initial iterations and in the later iterations the Monte Carlo estimate is used for several iterations before it is updated. For I-131, MCS was evaluated and compared with triple energy window (TEW) scatter compensation using simulation studies of a mathematical phantom and a clinically realistic voxel-phantom. Even after just two Monte Carlo runs, excellent agreement was found between the MCS estimate and the true scatter distribution. Accuracy and noise of the reconstructed images were superior with MCS compared to TEW. However, the improvement was not large, and in some cases may not justify the large computational requirements of MCS. Finally clinical application of MCS was demonstrated by applying the method to a radioimmunotherapy (RIT) patient study.**

I. INTRODUCTION

The loss of SPECT image quality and quantification accuracy due to photon scatter is well known. The various scatter compensation techniques developed in the past have been reviewed recently [1]. These methods can be grouped in to two broad categories: subtraction-based and reconstruction-based scatter compensation. In the subtraction-based approach the scatter component is estimated and subtracted from the projection data prior to reconstruction. The scatter estimate is typically obtained from multiple energy window acquisitions. In the reconstruction-based approach the scatter is included in the statistical model. With this approach there is no explicit subtraction of scatter counts, hence the noise increase associated with scatter subtraction methods is avoided. Comparative studies have shown that iterative reconstruction with accurate modeling of scatter is superior to pre-reconstruction scatter subtraction [2,3]. In the past Monte Carlo simulation has been used for accurate scatter modeling in 2D (Floyd et al [4]) and 3D (Beekman et al [5]) iterative SPECT reconstruction. The method of Floyd et al has massive computational requirements for pre-calculating and storing the full system matrix. Hence it was only implemented for 2D SPECT. Recently, because of computing advances the practical feasibility of this approach for 3D SPECT was re-investigated [6]. In the method of Beekman et al the scatter-modeling step involves the Monte Carlo calculation of low noise scatter projections. Their evaluations for Tc-99m imaging demonstrated that the reconstructions based on the Monte Carlo projector are superior to those based on an advanced analytical scatter model.

Our interest is in tumor and organ activity quantification for dosimetry in patients undergoing I-131 RIT for Non-Hodgkin's lymphoma. In I-131 SPECT, both object scatter and collimator scatter is highly significant because of the high energy of the photopeak (364 kev) and other emissions (637 kev, 722 kev). The goal of the present work was to implement highly accurate Monte Carlo based scatter modeling (MCS) with 3-D OSEM reconstruction. The SIMIND Monte Carlo algorithm [7], includes accurate physical modeling of the collimator (including collimator scatter and penetration) and has been extensively validated for I-131[8]. The latest version of SIMIND used in the present work has a newly developed collimator algorithm, which is based on the Delta scattering method [9]. Unlike in previous implementations of MCS [5] in the present approach the Monte Carlo scatter estimate is not used in the initial iterations and it is not updated at each iteration. The proposed method can be applied to clinical studies when a SPECT image and a co-registered attenuation map are available for defining the input object to the Monte Carlo projector. Co-registered CT derived attenuation maps are typically available for RIT patients at our clinic as they are used for SPECT attenuation correction. Although MCS has the potential for highly accurate scatter estimation it has high computational requirements to generate low noise scatter projections. In addition, this correction will not account for scattered photons that originated outside the SPECT camera field of view (FOV) because the input object to the projector does not extend beyond the FOV. Simpler multiple-energy window based methods may be able to correct for these scattered photons.

In this paper we discuss the implementation of MCS and carry out phantom studies to evaluate the method and compare it with a TEW scatter correction [10] used thus far in our clinical SPECT studies for I-131 RIT. Finally MCS is applied to a patient study to demonstrate clinical application. The present study does not focus on methods to speed-up the Monte Carlo projector or evaluate errors in the scatter model due to mis-registration and noisy attenuation maps.

Yuni K. Dewaraja is with the Department of Radiology, University of Michigan, Ann Arbor, MI 48109-0552 USA (e-mail: yuni@umich.edu).

Michael Ljungberg is with the Department of Medical Radiation Physics, Lund University, Lund, Sweden (e-mail: michael.ljungberg@radfys.lu.se)

Jeffrey A Fessler is with the Department of Electrical Engineering and Computer Science, University of Michigan, Ann Arbor, MI 48109 USA (e-mail: fessler@eecs.umich.edu).

I. METHODS

A. Reconstruction

In both TEW and MCS, the scatter estimate is included in the OSEM algorithm in the manner appropriate for Poisson statistics [11], i.e. scatter is included in the statistical model as a "known" additive term as shown below:

$$Y_i \approx Poisson\left\{ \sum_{j=1}^{n} g_{ij} x_j + s_i \right\} \qquad (1)$$

where x is the unknown image consisting of n voxels, Y is the measured projection data, G is the system matrix excluding scatter, and s is the scatter estimate. With scatter treated in this manner we include only attenuation and detector response in the forward/backprojector. This avoids the massive computational requirements associated with including scatter in the system matrix. Reconstruction was carried out with an unregularized multi-plane (3D) OSEM algorithm using 6 subsets.

In the TEW method, the photopeak window scatter counts for each pixel is estimated from counts acquired in two adjacent narrow subwindows following Gaussian smoothing (FWHM=3 pixels) of the subwindow projection data. This estimate is used in all iterations. In the MCS method, the TEW scatter estimate is used only in the initial iterations, until a reasonable reconstructed image is obtained. This initial reconstruction together with the phantom/patient attenuation map defines the input object to the SIMIND projector. Gaussian smoothing (FWHM=3 pixels) is performed on the SIMIND generated scatter estimate. To reduce noise, an analytical projector is used for the primary photons. In a previous study on SPECT reconstruction with Monte Carlo scatter compensation the scatter estimate was updated at each iteration [5]. This seems inefficient when iterative algorithms converge slowly. Therefore, in our implementation the MCS estimate is generated one time and is used for several iterations before recalculating a new estimate.

To investigate the number of photon histories needed to minimize noise we used 10^7, 10^8 and 10^9 photons/projection when generating the Monte Carlo scatter estimate. The run time for 10^7 and 10^8 histories was 2 hours and 20 hours respectively on a DEC ALPHA 1000 workstation. The simulation with 10^9 histories was carried out on multiple processors of the IBM POWER4+ system at the San Diego Supercomputer Center, University of California.

B. Phantom Simulations

Monte Carlo simulation was used not only to generate the scatter estimate during reconstruction but also to obtain the original projections. For the original phantom projections a large number (10^{10} photons/projection) of histories were simulated to generate essentially noise free projection data. Both a mathematical elliptical phantom and the anthropomorphic voxel-man phantom [12] were used. The elliptical tank was 23x31.5 cm and 20.5 cm in height and contained 2 hot-spheres (5.8 cm, and 2.9 cm diameter), one cold-sphere (5.8 cm diameter) and one warm-sphere (5.8 cm diameter) in a uniform background. The sphere to background activity concentration ratio for the hot spheres was 5:1 while that for the warm sphere was 1:2. For the voxel-man phantom, activity concentration ratios were assigned to reflect a typical situation in SPECT imaging after the therapy administration of I-131. To mimic the situation in patient imaging all 240 slices of the torso phantom were simulated, although only 60 of these slices were within the camera FOV. It is important to include all slices since photons originating outside the FOV that undergo scatter can contribute to the image.

A Picker Prism 3000 SPECT camera was modeled with a commercial ultra-high energy collimator (UHEGAP) that minimizes septal penetration. SPECT simulations employed 360 degrees, 60 angles a 20% photopeak at 364 keV, and two 6% adjacent scatter correction windows. For the elliptical phantom the matrix size was 64x64 with a pixel size of 7.2 mm while for the voxel-man the matrix was 128x128 with a pixel size of 4 mm.

C. Evaluation

In addition to visual comparison of images and profiles several image quality measures were calculated to quantitatively evaluate the scatter compensation. The normalized mean square error (NMSE) was calculated for both the scatter projections and for reconstructed images while the other measures were calculated for reconstructed images only.

The accuracy was evaluated using the NMSE defined by

$$\%NMSE = 100 * \left(\Sigma_i (x_i - p_i)^2 \right) \Big/ \Sigma_i p_i^2 \qquad (2)$$

where the sums are over a region of interest (ROI). When the NMSE is calculated for projection data, x represents the estimated scatter projection and p represents the true scatter projection. When NMSE is calculated for reconstructed data x represents the reconstructed image and p represents the true phantom. NMSE is computed for the noise free images.

For the spheres contrast was defined as

$$C = | l - b | / (l + b) \qquad (3)$$

where l and b are the count densities in the sphere and uniform background, respectively. Relative contrast is defined as the ratio of reconstruction contrast to true phantom contrast.

To measure noise, the original phantom projection data was scaled to 20 million total counts (this corresponds to a typical patient therapy scan in RIT) before the addition of Poisson distributed noise. The noise-free projection data and the noisy projection data were both reconstructed as described previously. The noise was measured using the normalized standard deviation (NSD) defined by

$$NSD = \sqrt{\Sigma_i (x_i - \bar{x}_i)^2 \Big/ N - 1} \left(\Sigma_i \bar{x}_i \Big/ N \right)^{-1} \qquad (4)$$

where the sums are over a ROI. Here, x is the image reconstructed from noisy data, $\bar{x}$ is the image reconstructed from noise free data and N is the number of pixels.

D. *Patient Study*

To demonstrate clinical application MCS compensation was applied to one patient in our I-131 RIT data archive. The lymphoma patient had been imaged 44 hours after therapy administration of 4Gbq of I-131 tositumomab using the same SPECT system modeled in the present phantom studies. The SPECT matrix size was 64x64 with a pixel size of 7.2 mm. The co-registered CT-derived attenuation map was available.

II. Results and Discussion

For MCS, the TEW estimate was used in the initial 20 iterations at which point the first Monte Carlo scatter estimate was generated. Below, MCS1 refers to the case where the first Monte Carlo scatter estimate was used in all further iterations (iteration 20 to 60) while MCS2 refers to the case where a second Monte Carlo scatter estimate was generated at iteration 40 and used for the next 20 iterations. Projection data was reconstructed 1) without scatter compensation 2) with TEW compensation 3) with MCS (both MCS1 and MCS2) compensation. The 'ideal' data set corresponding to primary (scatter-free) photons was also simulated and reconstructed without scatter compensation. All the reconstructions included attenuation correction and 3D detector response modeling.

A. *Elliptical phantom*

For the scatter projections, the NMSEs for the TEW estimate and MCS estimates with different numbers of photon histories are compared in Table 1. Based on these results it is evident that 10^7 photons/projection is too few histories for generating an accurate Monte Carlo scatter estimate. With both 10^8 and 10^9 photons/projection the NMSE values for MCS

TABLE I
NMSE CALCULATED FOR PROJECTION DATA.

	TEW	MCS1			MCS2	
		10^7	10^8	10^9	10^8	10^9
%NMSE	1.5	8.3	1.3	1.1	0.6	0.3

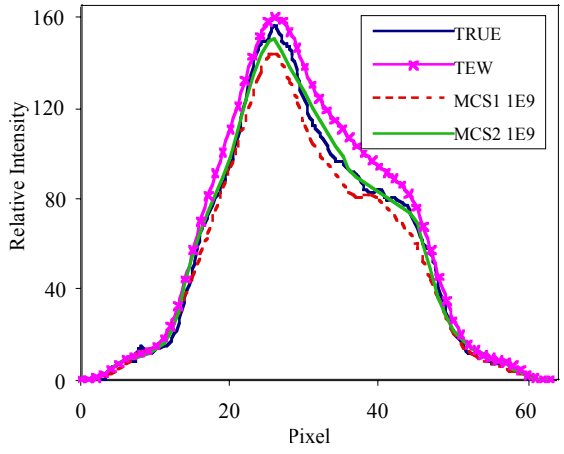

Fig 1. Profile across a typical scatter projection.

are better than that for TEW. Figure 1 shows the profile across a typical scatter projection. There is good agreement between MCS and the true scatter profile while TEW consistently overestimates the scatter. Because of the almost perfect agreement between the true scatter profile and MCS2 it appears that further updating of the scatter estimate is not necessary. Note that in Figure 1, the profiles corresponding to the scatter estimates are smoother than that corresponding to the true scatter because as described previously Gaussian smoothing was applied to the estimates.

The NMSE calculated for the reconstructed images initially decrease with iteration, but then increases with iteration due to noise. For the large hot sphere, the plot of NMSE versus iteration for the different reconstructions is shown in Figure 2. For the different reconstructed images the minimum NMSE values for the total image and the sphere ROIs are given in Table 2. The results of Table 2 and Figure 2 shows that both scatter modeling methods significantly improve the NMSE when compared with images reconstructed without scatter correction. The NMSE values for MCS with both 10^8 and 10^9 photons/projection are superior to those for TEW, however the improvement is not very large. Note that because the NMSE is defined relative to the true phantom it includes not only scatter effects, but resolution effects as well. This explains why values for scatter corrected images can be superior to those of the primary images.

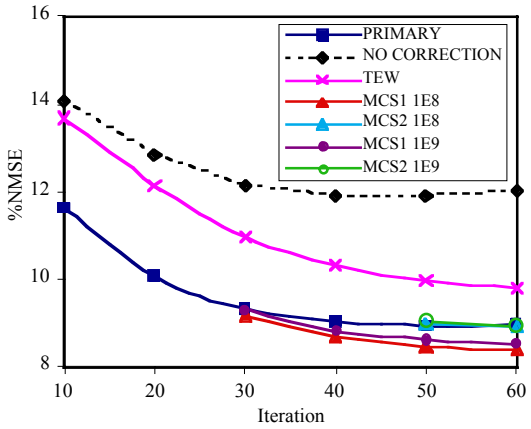

Fig 2. %NMSE versus iteration for the hot sphere ROI.

TABLE II.
MINIMUM %NMSE FOR THE DIFFERENT RECONSTRUCTIONS.

	Primary	No corr.	TEW	MCS	
				10^8	10^9
Total image	8.9	22.7	9.5	9.5	9.5
Large hot sphere	9.0	11.9	9.8	8.4	8.6
Small hot sphere	15.1	8.4	15.2	13.7	13.7

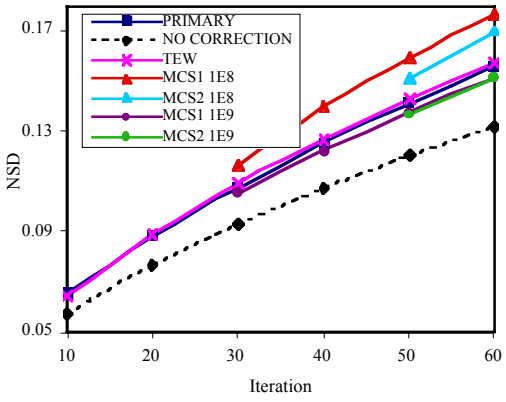

Fig 3. NSD versus iteration for the total image.

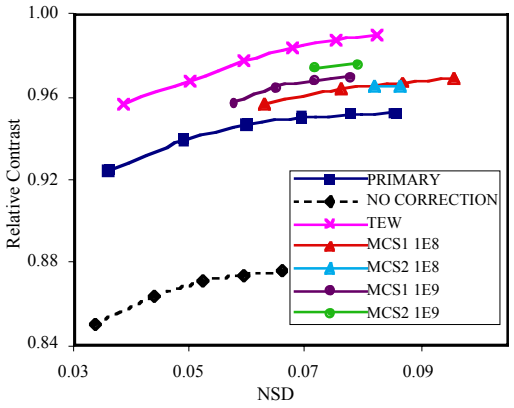

Fig 4. Contrast versus NSD for the large hot sphere.

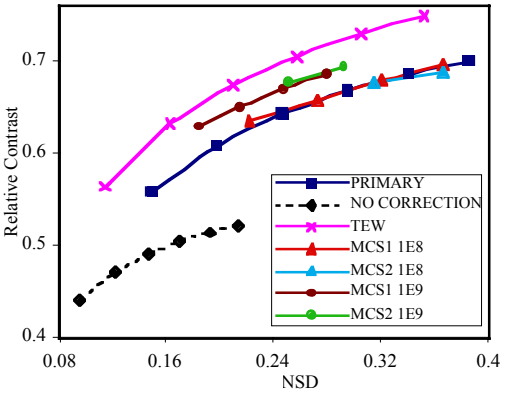

Fig 5. Contrast versus NSD for the cold sphere.

For the total image, NSD is plotted as a function of iteration for the different reconstructions in Figure 3. NSD values for MCS are slightly superior to TEW when 10^9 photons/projection are used while it is slightly inferior when 10^8 photons/projection are used. Contrast-to-noise curves for the hot and cold spheres are plotted in Figures 4 and 5. Again, both scatter modeling methods significantly improves the contrast-to-noise curves compared with images reconstructed without scatter correction. The curve for TEW appears superior to that of MCS as well as that of the primary data. However, this is because the TEW method overcompensates for scatter, which is also evident from the scatter profiles of Figure 1.

B. Voxel-man phantom

For the voxel phantom the profiles across a typical scatter projection are shown in Figure 6. As for the elliptical phantom, the profiles show that TEW overestimates scatter while there is almost perfect agreement between the true scatter profile and the second MCS estimate. The %NMSE calculated for the scatter projections were 1.9 for TEW, 3.3 for MCS1 and 1.2 for MCS2. The MCS estimate is more accurate than the TEW estimate despite the fact that TEW can account for scattered photons that originate from voxel-man slices outside the camera FOV. For the reconstructed images, the NMSE was calculated for the total image only and are plotted as a function of iteration in Figure 7. Both TEW and MCS significantly improve NMSE compared with images reconstructed without scatter correction. The NMSE values for MCS are slightly superior to those for TEW. Figure 8 shows one slice of the voxel phantom activity and attenuation maps and the reconstructed images at iteration 60. The figure clearly shows the degradation in contrast when no scatter correction is used. Both the TEW and MCS corrected images look very similar to the image corresponding to the scatter-free data.

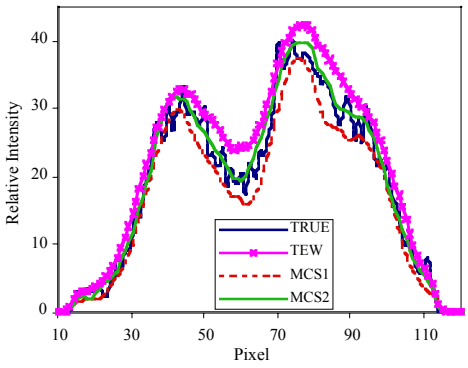

Fig 6. Profile across a scatter projection of voxel-man.

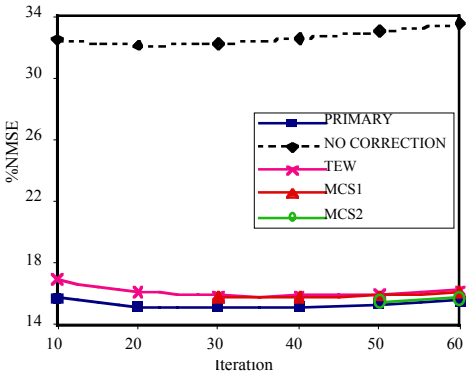

Fig 7. %NMSE versus iteration for the total image of the voxel-man.

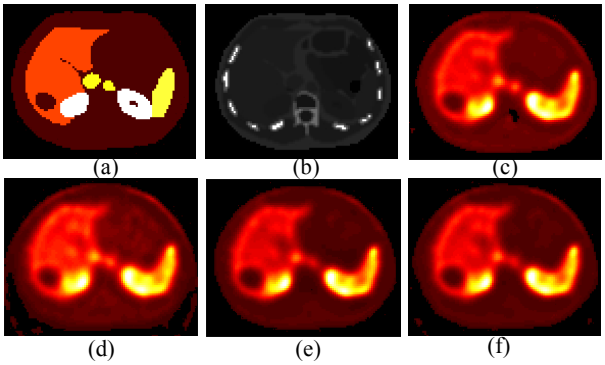

Fig 8. Slice of voxel-man (a) activity map (b) attenuation map (c) reconstructed image corresponding to primary photons (d) image reconstructed without scatter correction (e) image reconstructed with TEW (f) image reconstructed with MCS.

C. Patient study

The SPECT reconstruction with TEW at iteration 20 and the patient attenuation map defined the input object to the Monte Carlo projector (a typical slice of the input object is shown in Figure 9). As in the phantom studies the first MCS scatter estimate was used for iterations 20 to 40 at which point a second MCS estimate was generate and used for iterations 40 to 60. MCS estimates were generated using 10^9 photons/projection. Figure 10 shows the comparison between the TEW and MCS2 estimates for a typical scatter projection. For the patient the true scatter is not known, but as in the phantom TEW overestimates scatter compared with MCS. Based on the results for the phantom studies we can expect the MCS estimate to be more accurate than the TEW estimate.

III. CONCLUSION

These studies demonstrate highly accurate scatter compensation with MCS, even after just two updates of the Monte Carlo estimate. MCS outperformed TEW in terms of NMSE and noise, but the improvement was not large, and in some cases may not justify the large computational requirements of MCS. The TEW corrected images had higher contrast compared with MCS because of overcorrection for scatter. MCS image accuracy was not significantly improved by using more than 10^8 photons/projection. Clinical applicability of the method was demonstrated by the patient study, where as in the phantom studies TEW overestimated the scatter compared with MCS. The SIMIND simulation time to generate the scatter estimate was relatively long (20 hours on a workstation for 10^8 photons/projection). However, in the present implementation the MCS estimate is not updated at each iteration, therefore the speed of the Monte Carlo simulator is less important than in previous implementations.

IV. ACKNOWLEDGMENT

This work was supported by grant R01 EB001994 awarded by the NIH, US Department of Health and Human Services. Computing resources provided by NPACI at the San Diego Supercomputer Center is acknowledged.

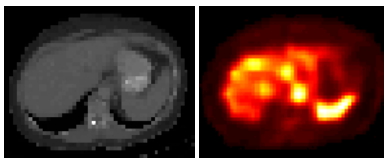

Fig 9. One slice of the patient attenuation map and SPECT activity distribution used as input to the Monte Carlo projector.

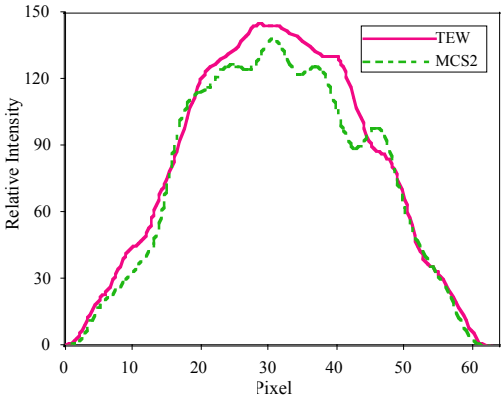

Fig 10. Profile across a scatter projection for the patient.

V. REFERENCES

[1] Zaidi H and Koral K. Scatter modeling and compensation in emission tomography. Eur J Nucl Med Mol Imaging 2004;31:761-782.

[2] Frey et al. A comparison of scatter compensation methods in SPECT: subtraction based techniques versus iterative reconstruction with accurate modeling of the scatter response. *IEEE Nucler Science Symposium and Med Imag Conf, Conference Record*, 1993.

[3] Beekman FJ, Kamphuis C, Frey EC. Scatter compensation methods in 3-D iterative SPECT reconstruction: A simulation study. *Phys Med Biol.* 1997;42:1619-1632.

[4] Floyd CE, Jaszczak RJ, Greer KL, Coleman RE. Inverse Monte Carlo as a unified reconstruction algorithm for ECT. *J Nucl Med*, 1986;27:1577-1585.

[5] Beekman FJ, de Jong WAM, van Geloven S. Efficient fully 3-D iterative SPECT reconstruction with Monte Carlo based scatter compensation. IEEE Trans Med Imag, 2002;21:867-877

[6] Buvat I, Lazaro D, Breton V. Fully 3D Monte Carlo reconstruction in SPECT: proof of concept and is that worthwhile? Conference proceedings of the VII th International Meeting on Fully three-dimensional Image Reconstruction in radiology and Nuclear Medicine, June 2003, Saint-Malo, France.

[7] Ljungberg M, Strand S-E. A Monte Carlo program simulating scintillation camera imaging. *Comp Meth and Progr in Biomed*. 1989;29:257-272.

[8] Dewaraja YK, Ljungberg M, Koral KF, Accuracy of I-131 tumor quantification in radioimmunotherapy using SPECT imaging with an ultra-high-energy collimator: Monte Carlo study, *J Nucl Med*. 2000;41:1760-1767.

[9] Ljungberg M, Larsson A, Johansson L. A new collimator simulation in SIMIND based on the Delta-scattering technique. *IEEE Nucler Science Symposium and Med Imag Conf, Conference Record*, Rome, 2004.

[10] Ogawa K, Harata Y, Ichihara T, Kubo A, Hashimoto S. A practical method for position dependent Compton scatter compensation in single photon emission CT. *IEEE Trans Med Imag*. 1991;10:408-412.

[11] Bowsher J, Johnson V Turkington T et al. Bayesian reconstruction and use of anatomical a priori information for emission tomography. IEEE Trans Med Imag. 1996;15:673-686

[12] Zubal IG, Harrell CR, Smith EO, Rattner Z, Gindi G, Hoffer PB. Computerized three-dimensional segmented human anatomy. *Med Phys*. 1994;21:299-302.